Journal Pre-proof

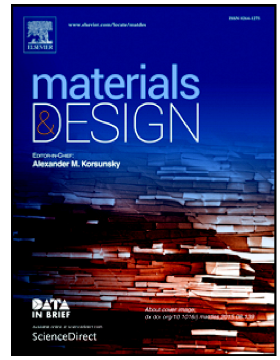

Experimental and simulation investigation on thermal-vibratory stress relief process for 7075 aluminium alloy

Hanjun Gao, Shaofeng Wu, Qiong Wu, Bianhong Li, Zihan Gao, Yidu Zhang, Shuai Mo

PII: S0264-1275(20)30488-3

DOI: https://doi.org/10.1016/j.matdes.2020.108954

Reference: JMADE 108954

To appear in: *Materials & Design*

Received date: 2 June 2020

Revised date: 22 June 2020

Accepted date: 3 July 2020

Please cite this article as: H. Gao, S. Wu, Q. Wu, et al., Experimental and simulation investigation on thermal-vibratory stress relief process for 7075 aluminium alloy, *Materials & Design* (2020), https://doi.org/10.1016/j.matdes.2020.108954

This is a PDF file of an article that has undergone enhancements after acceptance, such as the addition of a cover page and metadata, and formatting for readability, but it is not yet the definitive version of record. This version will undergo additional copyediting, typesetting and review before it is published in its final form, but we are providing this version to give early visibility of the article. Please note that, during the production process, errors may be discovered which could affect the content, and all legal disclaimers that apply to the journal pertain.

© 2020 Published by Elsevier.

Experimental and Simulation Investigation on Thermal-vibratory Stress Relief Process for 7075 Aluminum Alloy

Hanjun Gao[1], Shaofeng Wu[1,2], Qiong Wu[1]*, Bianhong Li[3], Zihan Gao[1], Yidu Zhang[1], Shuai Mo[4]

1. State Key Laboratory of Virtual Reality Technology and Systems, School of Mechanical Engineering and Automation, Beihang University, Beijing, 100191, PR China;
2. Key Laboratory of Advanced Manufacturing Technology, Beijing University of Technology, Beijing, 100124, PR China;
3. School of Mechatronical Engineering, Beijing Institute of Technology, Beijing City, 100081, P R China;
4. School of Mechanical Engineering, Tianjin Polytechnic University, Tianjin, 300387, PR China;

***Corresponding author:** Qiong Wu, wuqiong@buaa.edu.cn; Tel.: +86-10-8231-7756/+86-134-6661-7275;

Abstract: Residual stresses evidently affect the strength, fatigue property and machining deformation of the mechanical components. Therefore, stress relief processes are extensively applied in the manufacturing to enhance the mechanical properties of products. In this study, seven 7075 aluminium alloy specimens are treated by thermal- vibratory stress relief (TVSR), thermal stress relief (TSR), and vibratory stress relief (VSR). Finite element (FE) models considering the stress relaxation effects and transient periodic vibration loads are proposed to simulate the TVSR, TSR and VSR process. The residual stresses before and after the processes are measured and compared, and the effectiveness of the FE models is validated. Scanning electron microscope (SEM) and transmission electron microscope (TEM) are used to observe the microstructure and crystal dislocation, respectively. Results show that TVSR can evidently reduce the residual stress in aluminum alloy, and the stress relief rate of TVSR for the peak stress are 20.43% and 38.56% higher than that of TSR and VSR, respectively. It also found that TVSR has no obvious influence on the grain size, but evidently increase the dislocation density. Eventually, the stress relief mechanism of TVSR is analyzed and summarized.

Keywords: thermal-vibratory stress relief; residual stress; FEM; dislocation density; stress relaxation;

Graphical Abstract

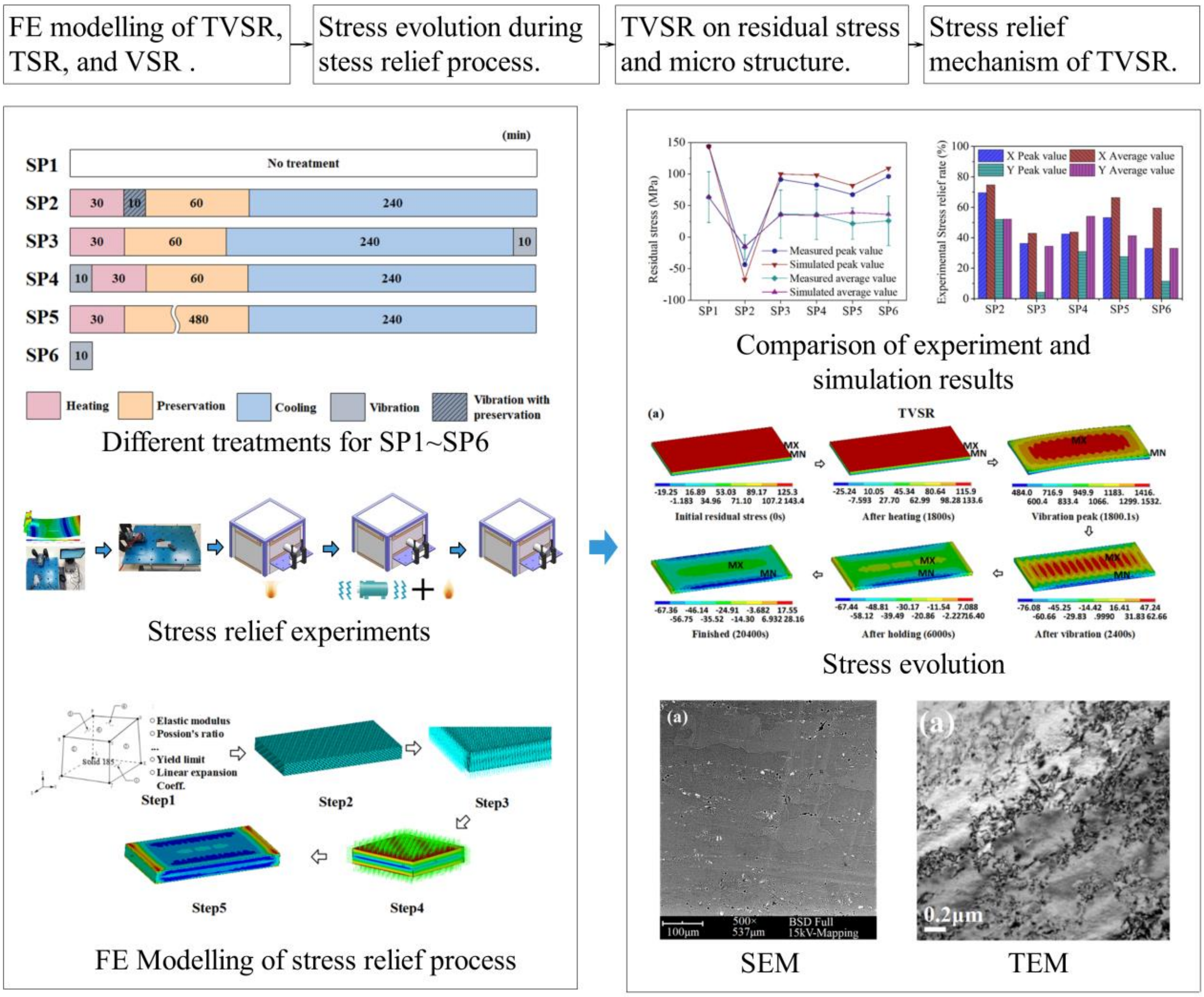

1. Introduction

Residual stresses originate from the elastic accommodation of misfits between different regions in a structure [1]. It is inevitably produced in the course of manufacture due to the uneven temperature and stress field [2]. The strength [3], fatigue property [4] and machining deformation [5] are significantly affected by the residual stress. Therefore, the stress control processes are extensively applied in the manufacturing to enhance the mechanical properties of the structural components.

Most metallic materials are vulnerable to the tensile load and relatively invulnerable to compressive stress. Consequently, in most cases, the compressive residual stress is advantageous to the mechanical properties, while the tensile stress is disadvantageous. As a result, in order to enhance the mechanical and metallurgical properties, some specific processes, e.g. shot peening (SP), severe shot peening (SSP), laser shock peening (LSP), and rolling, are utilized to induce the compressive stress [6].

The influences of the aforementioned processes on the residual stress evolution and microstructure arise extensive attentions of the researchers. Vázquez et al. [7] found that SP can significantly enhance the fretting fatigue of Al 7075-T651. The effect of LSP is also notable, but less than that produced by SP in most cases. Zhu et al. [8] proved that the effects of SP on the CNT/6061 composite are distinct. Wu et al. [9] investigated the influence of multiparameter SP on the residual stress distribution of SiCp/2024Al using finite element (FE) models and experiments. Atig et al. [10] presented a probabilistic method to obtain the variation of the induced residual stress profile and the Almen intensity by considering the dispersivity of the key process parameters. Sorsa et al. [11] applied the surface Barkhausen noise to measure the stress distribution generated by SP, and they found that the influence layer depth of the residual stress is less than 0.5mm.

Some researchers proposed analytical and numerical calculation models to investigate the residual stress evolution in the SP process. Ghasemi et al. [12] developed a FE model to evaluate the SP coverage on the surface state by considering the influences of element size, Rayleigh damping, and target plate size on residual stress distribution. Mahmoudi et al. [13] presented the comprehensive numerical and experimental study on the influence of original residual stresses on the SP sample. Tan et al. [14] proposed a calculation model using a sinusoidal decay function to study the induced compressive residual stress after SP. Sherafatnia et al. [15] proposed a calculation model using elastic–plastic evaluation and Hertzian contact theory to investigate the residual stress evolution during impingement and rebound stages of SP. Martín et al. [16] analyzed the residual stress relaxation of Al 7075-T651 produced in fretting fatigue tests and the effect of SP on the surface roughness by presenting a fretting fatigue life model.

SSP, which uses more intense strength compared to conventional SP, can have better residual stress and mechanical property control effect than general SP in some circumstances. Bagherifard et al. [17] found that notwithstanding the cast iron specimen has high surface roughness due to high energy impacts, and SSP has better effects in fatigue strength improvement. Trško et al. [18] detected an obvious increase in fatigue life of 50CrMo4 steel in the ultra-high cycle region after SSP surface treatment because of the variation of the grain size and residual stress distribution. Hassani-Gangaraj et al. [19] proposed a FE model of SSP to calculate the resultant gradient of grain size in the surface.

LSP is a new technique that is already being deployed widely for residual stress control and surface strengthening. Ahmad et al. [20] discovered that the use of ablative tape increases the surface compressive stress of marine steel welds after LSP, and the influencing depth increases with the number of peening layers. Chen et al. [21] detected that multiple SP is advantageous to increase the influence layer depth of high compressive residual stress in Sandvik Austenite and Ferrite 2507 duplex stainless steel. The maximum compressive residual stress of surface and 10 μm depth reaches −1070.5 MPa and −910.5 MPa after triple SP, respectively. Sun et al. [22] found that the grain size decreases from 60 to 47 μm after LSP, and the initial tensile residual stresses are turned into compressive stress.

Besides, the rolling process is also an alternative for inducing the stress and microstructure adjustment. Coules et al. [23] found that the rolling can turn the unsatisfactory tensile stresses into large compressive stress of S355JR structural steel. Zhang et al. [24] proposed an approach for effective enlargement of compressive residual stress field using ultrasonic surface rolling process with the association of both the static and dynamic loads. Colegrove et al. [25] designed the “profiled” and “slotted” rollers for high-pressure rolling to eliminate the residual stress and distortion generated by wire and arc additive manufacture (WAAM) process. Beghini et al. [26] conducted the deep rolling process with a carbide roller with conical and rounded contact to reduce the residual stress and distortion of AL7075-T6 aluminium alloy.

Above processes (SP, SSP, LSP and rolling) can generate the compressive stress on the material surface through the external impact or extrusion loads, as a result, the strength, hardness, and fatigue life are improved. However, only the stress state on the surface can be affected by these processes. In many cases, the stress relief processes, such as TSR, VSR, deep cryogenic treatment (DCT) and ultrasonic stress relief (USR), are applied to comprehensively control the surface and internal residual stresses.

TSR is the most mature and widely used stress relief process. Rahimi et al. [27] investigated the tensile stress relaxation behaviors at elevated temperatures used for aging heat treatments. Zeng and Bieler [28] investigated the influences of TSR on the microstructure, crystal structure, and residual stress evolution of α, α', α" and β phase Ti6Al4V. Luo et al. [29] analyzed the aging mechanism of aluminium alloy using first principle calculation method and comprehensively evaluated the effects of TSR on the residual stress / strain. Sun et al. [30] proposed a multistage interrupted TSR method for eliminating residual stresses of Al–Zn–Mg–Cu alloy and validated the progressiveness of the method by experiments.

Song et al. [31] found that the grains of selective laser melting (SLM) iron parts are refined after TSR because of the residual stress redistribution. Hönnige et al. [32] observed that 300-400 MPa residual stresses of friction stir welds (FSW) Ti-6Al-4V alloy are decreased to a negligible level after treated by a 760 °C for 45 minutes TSR.

Heat treatment under high temperature is not the only way to eliminate the residual stress. It is found that artificial low temperature treatment also has good stress relief effect. Senthilkumar [33] demonstrated that DCT with −196 °C for 24 h enhances ultimate tensile strength by 33.94% and significantly increases the compressive residual stress. Xu et al. [34] summarized that residual stresses of Ti–6Al–4V joints are declined by 17.2%–46.5% in different directions after DCT for 24 hours. Ko et al. [35] employed the Zener-Wert-Avrami function to investigate the relaxation of residual stress of 6061 aluminum alloy caused by the DCT.

VSR is also a very concerned stress relief process. There are plenty of the researches on VSR and its influences on the stress relief and material mechanical properties. Wang et al. [36] discovered that VSR is effective to the stress concentration zone of cold-rolled AZ31 Mg alloys, rather than all residual stresses. Ebrahimi et al. [37] demonstrated that by increasing the VSR applied load frequency up to 95% of the natural frequency (NF), the longitudinal residual stress of AZ31 Mg alloys is decreased more than 80%. Gao et al. [38] detected that VSR can significantly decrease the residual stress in 7075 aluminium alloy, and the fatigue life increases by 11.11% after VSR with 0.04mm vibration amplitude. And they also [39] studied the influences of VSR and TSR on the residual stress and fatigue properties of Ti6Al4V. Gong et al. [40] found that the dimensional stability of aluminum alloy thin-walled parts can be evidently increased by VSR. Vardanjani et al. [41] presented a theoretical model on the basis of the linear kinematic hardening theory to investigate the stress relief mechanism of VSR. Mohanty et al. [42] improved the VSR process using an electromagnetic exciter, and results showed that the residual stress with the mean value of 100MPa is eliminated from the AISI 316 welded specimens.

Besides, Shalvandi et al. [43] believed the residual stress of the 316 stainless steel Almen strips can be reduced about 40% by TSR, while that is reduced about 36% by USR. Gu et al. [44] developed an ultrasonic vibration plasticity model on the basis of the dislocation glide kinetics theory, and reduced the residual stress in AISI 1045 steel using USR.

TSR and VSR have their own advantages and disadvantages, and the stress relief mechanisms are quite different. TSR can homogenize the uneven microstructure and residual stress field through the annealing treatment for hours. The stress is relieved because of the stress relaxation and the reduction of material yield limit at higher temperatures. The residual stress treated by TSR has good uniformity. However, TSR is time-consuming and energy-consuming, and it could change the microstructure and decrease the material mechanical properties. Compared with TSR, VSR is a more high-efficiency and energy-conservation stress relief process. Generally, VSR takes no more than 1 hour. Because VSR is conducted under the one of the natural frequencies, the generated dynamic stress under resonance condition is unevenly distributed in the workpiece. Thus, the stress reduction varies with the position in the specimen.

Lv and Zhang [45] proposed a thermal-vibratory stress relief (TVSR) to enhance the stress-relief effect of the existing process. Results showed that the stress relief ratio of TVSR is 42.5% higher than that of VSR. Li et al. [46] applied TVSR to reduce the residual stress of 50mm thick DH 36 steel welded plates. Chen et al. [47] compared the stress relief effect of TSR, VSR and TVSR using twelve 2219 aluminum alloy welding specimens. They found that the TSR is more effective to the weld direction, but it is less effective to the perpendicular direction. TVSR performed well in both directions.

Although some researches on TVSR have been conducted, as a novel stress relief process, the stress relief mechanism, coupling mode of heat and vibration, and its influences on the microstructure and stress revolution still need further exploration. Moreover, the existing FE model for heat treatment is mainly used to simulate the stress generation and phase transition process [48,49], but the FE model considering the stress relaxation effect for simulating the stress relief process of TVSR and TSR is rarely reported. In this study, the specimens taken from 7075 aluminium alloy forging plates are treated by TSR, VSR, and TVSR under different process parameters. The corresponding FE models of TSR, VSR and TVSR process are established to further study the stress evolution and stress relief mechanism. The residual stresses before and after the treatments are measured, and SEM and TEM are used to characterize the microstructure and crystal dislocation, respectively. Eventually, the influences of TVSR on the residual stress, microstructure, and crystal dislocation are analyzed, and the stress relief mechanism of TVSR is summarized.

2. Experiments and simulations

2.1 Stress relief experiments

2.1.1 Equipment and specimens

TVSR experiments are conducted using the stress relief experiment platform (SREP) produced by Beihang University (Beijing, China). SREP consists mainly of two parts: the vibration and heating system (**Fig.** 1). The vibration system includes the exciter, fixture, acceleration sensor, vibration table, vibration isolation pad, and vibration controller, and the heating system includes temperature controller, bottom bracket, cover, insulation board, heating device, and temperature sensor.

Journal Pre-proof

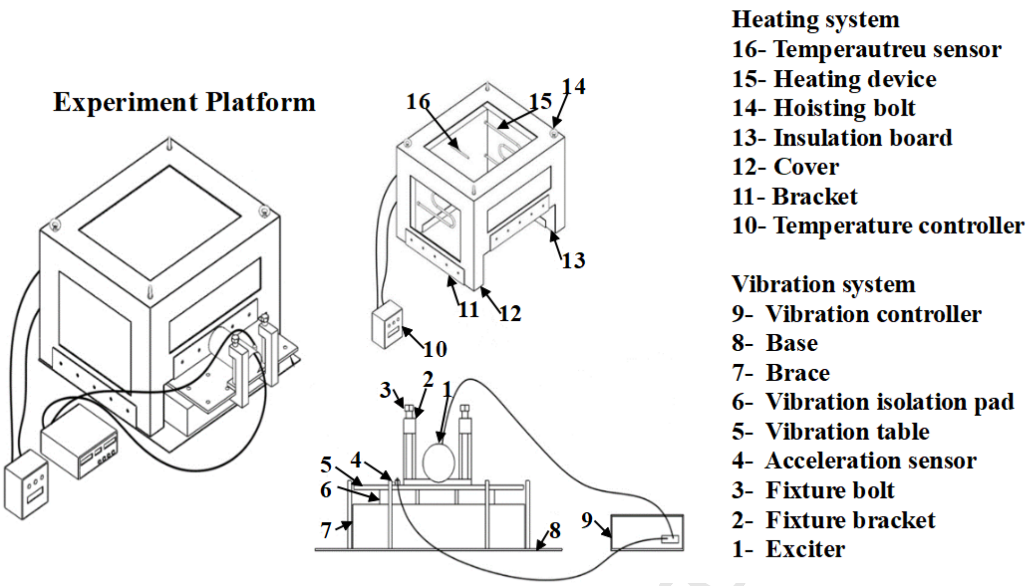

Fig. 1 The schematic diagram of stress relief experiment platform (SREP).

Seven cuboid specimens (SP1~SP6) are taken from a 7075-T6 aluminium alloy forging plate for the stress relief experiments, and the chemical composition is shown in **Tab.** 1. Plane milling is used to machine the oxide layer on the surface. The size of each specimen is 200mm×100mm×20mm. Residual stresses of 2mm depth beneath the specimen surface is measured and monitored to investigate the stress relief effects of TVSR. The general process of TVSR is shown in **Fig.** 2.

Tab. 1. Chemical composition of 7075-T651 aluminium alloy (%).

Alloy	Si	Fe	Cu	Mn	Mg	Cr	Ni	Zn	Ti	Al
7075	0.40	0.50	1.2–2.0	0.30	2.1–2.9	0.18–0.28	0.05	5.1–6.1	0.20	Bal

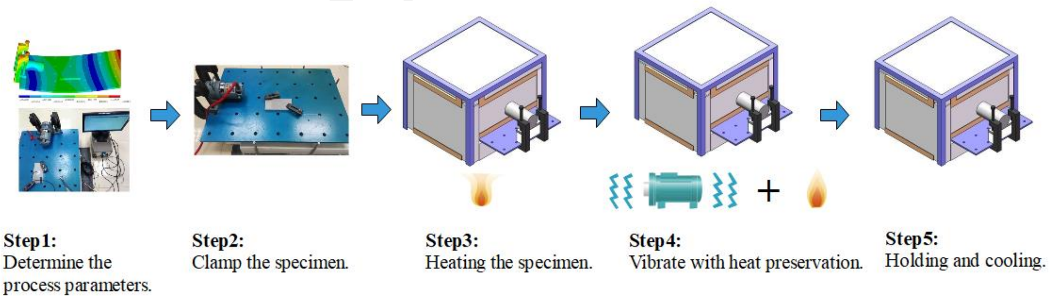

Fig. 2 General process flow of TVSR.

2.1.2 Determination of experimental parameters

Modal analysis is conducted to obtain the natural frequency of vibration system with the specimen using ANSYS software. The exciter, which is an eccentric motor with 0~4000Hz excitation frequency, is modeled as a mass element in the FEM modeling, and four sets of spring elements with three directions are used to model the connection between the vibration table and the ground. 3D Solid elements are applied to model the specimen and vibration table. The finite element model is presented in **Fig.** 3.

Journal Pre-proof

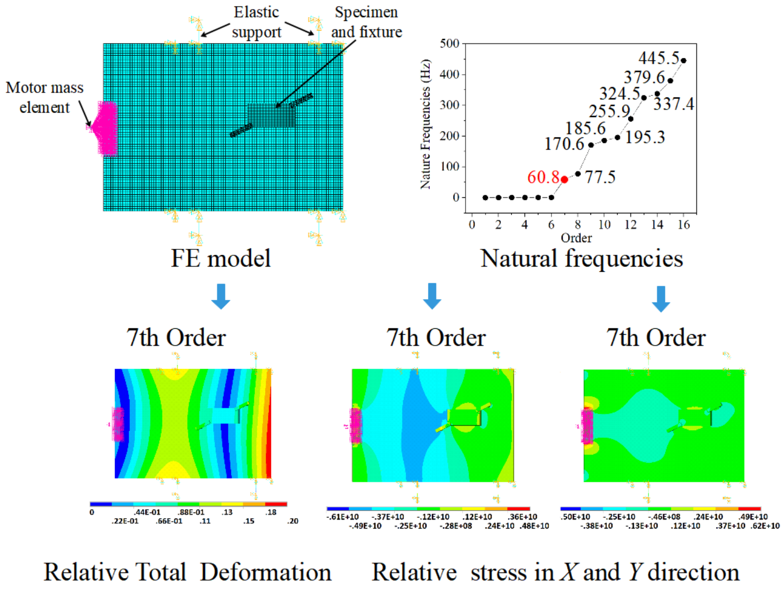

Fig. 3 Finite element (FE) model of the vibration system and 7_{th} order modal analysis results.

The 1_{st} to 16_{th} order natural frequencies and modal results are obtained from the calculation results, which are shown in **Fig.** 3. It shows that the first six order NFs are closed to 0 Hz, because the vibration table is freely placed on the vibration isolation pad. Hence, the 7_{th} order is the actual 1_{st} order NF of the vibration system, and other actual NFs can deduce the rest from this. The 1_{st} order NF (fundamental frequency) is generally taken as the vibration frequency of VSR [36], therefore, the vibration frequency of TVSR in present study is determined as 60.8Hz. The stress relief occurs in the first several minutes of VSR, as a result, the vibration duration in this paper is set as 10 minutes.

Moreover, the heat holding temperature and duration of 7075-T6 aluminium alloy TSR are 175°C and 6~8 hours, respectively [38]. TVSR needs much less time than TSR. Thus, the holding temperature and duration of TVSR is set as 175°C and 1 hour, respectively.

2.1.3 TVSR experiments

In the light of the experiment parameters determined in Section 2.1.2, seven specimens are treated by different stress relief processes: SP1 is set as the control specimen, namely, no treatment is conducted; SP2 is treated by TVSR; SP3 is first treated by TSR for 1 hour, then by VSR; SP4 is first treated by VSR, then by TSR for 1 hour; SP5 is treated by TSR; SP6 is treated by VSR. Detailed process parameters and flows are shown in **Fig.** 4. The specimen and equipment of TVSR experiment is presented in **Fig.** 5.

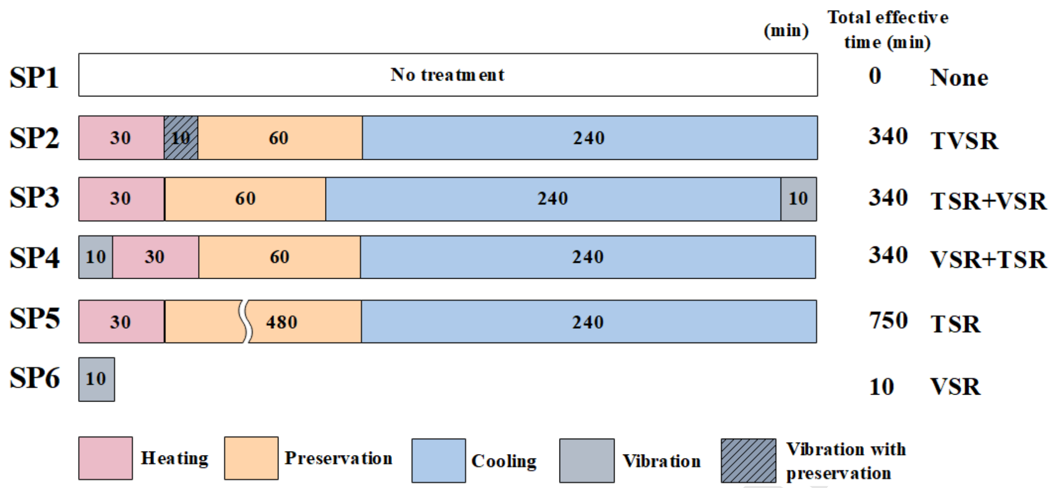

Fig. 4 Detailed process parameters and flows of SP1~SP6.

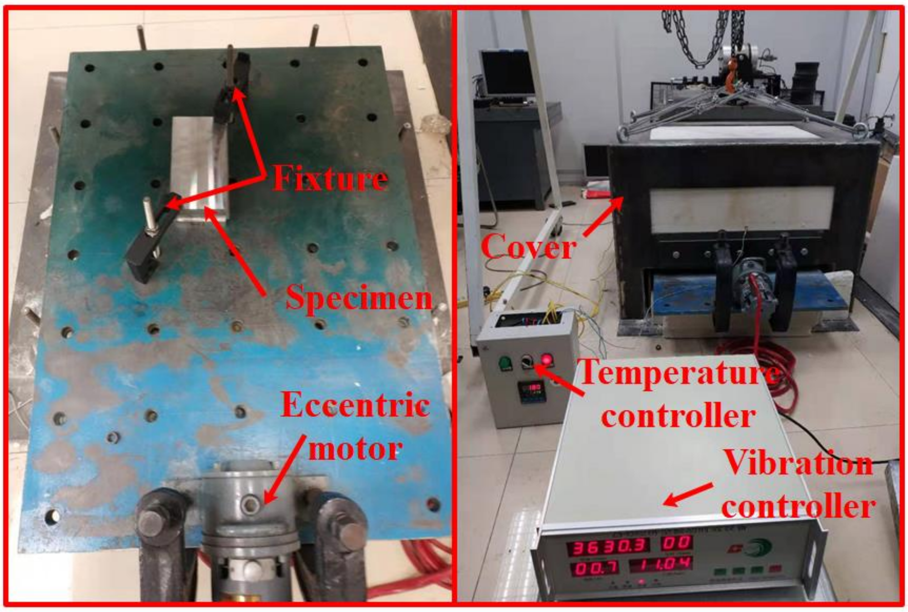

Fig. 5 Specimen and equipment of TVSR experiment.

2.2 FE Simulations for stress relief processes

The residual stress is released in TSR process due to the stress relaxation and the decrease of the elastic modulus and yield limit. The stress relaxation process can be simulated using Strain Hardening Implicit Creep Equations [50] in FE simulations,

$$\dot{\varepsilon} = C_1 \sigma^{C_2} \varepsilon^{C_3} e^{-C_4/T} \tag{1}$$

where ε is the creep strain, $\dot{\varepsilon}$ is the creep stain rate, σ is creep stress, T is the temperature, and C_1~C_4 are the constant coefficients.

C_1~C_4 can be determined by the stress relaxation tests under four different stress levels. Therefore, the stress relaxation tests are conducted at 175°C using RD-50 high-temperature creep endurance testing machine (produced by Changchun Kexin Instrument Co., Ltd, China). The shape and size of the specimens are presented in **Fig.** S1, and the experimental equipment is shown in **Fig.** S2. The stress relaxation tests are performed under 50, 100, 150 and 250 MPa stress levels. The raw and fitted data of stress relaxation tests are shown in **Fig.** 6, and a nonlinear equation set consists of four equations are established based on the test results and **Eq.** (1), taking the constant coefficients C_1~C_4 as the unknowns.

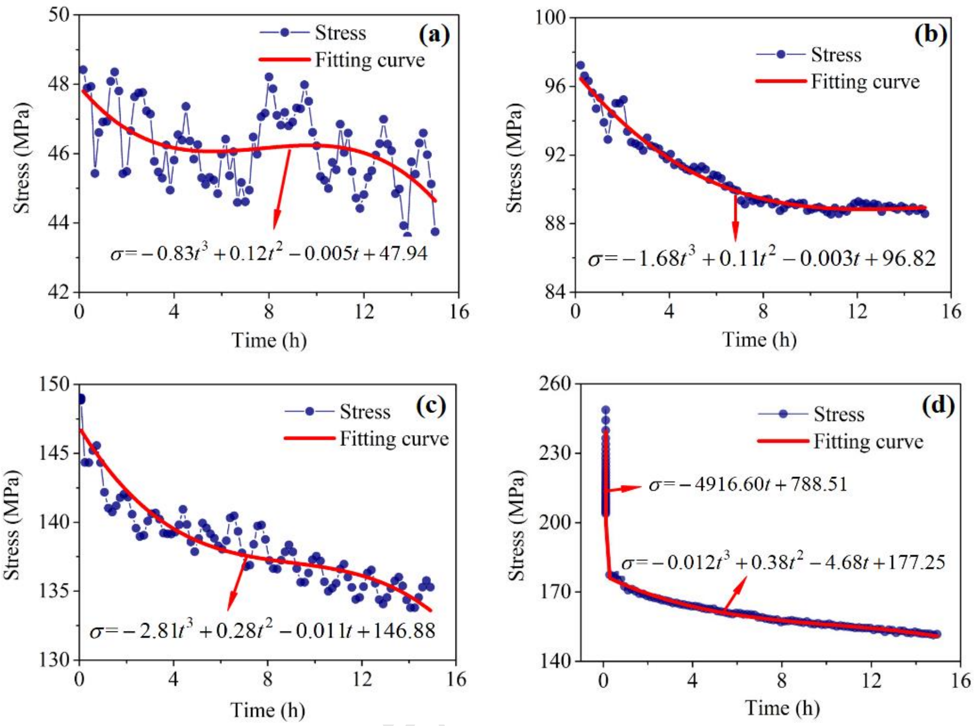

Fig. 6 Stress relaxation curves of 7075 aluminium alloy at 175°C under (a) 50MPa, (b) 100MPa, (c) 150MPa and (d) 250MPa.

The C_1~C_4 are obtained by solving the four nonlinear equations, and results are $C_1=2.13\times10^{-14}$, $C_2=3.40$, $C_3=0.14$, and $C_4=404.54$.

The periodic force or displacement boundary conditions, which causes the dynamic stress in TVSR or VSR process, are applied to the FE models to simulate the periodic vibration process. To improve the convergence and efficiency of the model, the displacement boundary conditions are utilized in this study, and the displacement amplitude should be determined first.

Before TVSR and VSR simulation, the harmonic analysis is carried out to determine the vibration amplitude of the specimen based on the FE model of SREP in Section 2.1.2. A sinusoidal exciting force, which is generated by the eccentric motor, is applied to the mass element of the eccentric motor (as is shown in **Fig.** 3). The amplitude of exciting force F can be calculated by the Eq. (2) [51]:

$$F = me\omega^2 \tag{2}$$

where m is the mass of the eccentric motor, e is the eccentricity, and ω is circular frequency of the 7_{th} natural frequency. In this study, m=21kg, $\omega=2\pi f=2\times3.14\times60.8=381.8$rad/s, and e=1.5mm. Thus, the calculate result of exciting force is 4600N.

Hence, the displacement amplitude of the specimen under 4600N exciting force can be obtained using harmonic analysis in ANSYS software. The calculated displacement amplitudes of typical points on the specimen surface are shown in **Fig.** 7. The displacement amplitudes at 60.8Hz (resonance frequency) are extracted as the periodic displacement boundary conditions in the following TVSR or VSR simulations.

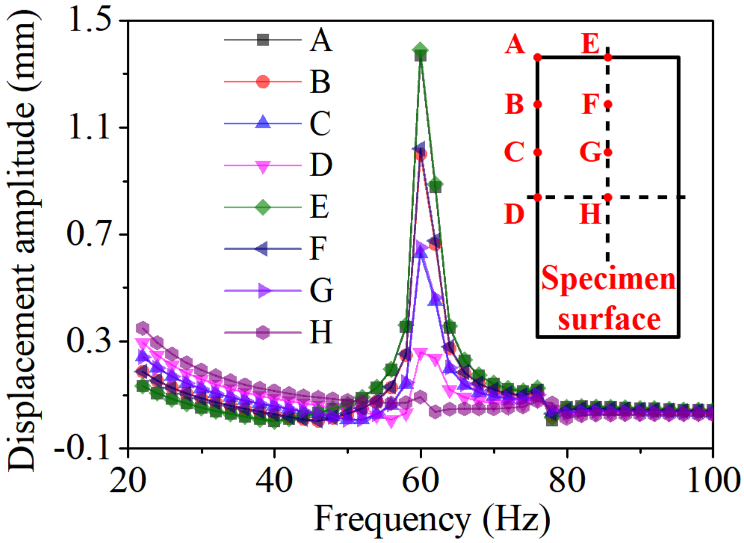

Fig. 7 Displacement amplitudes of the typical points on the specimen surface.

Thus, the thermal-mechanical coupling FE models of stress relief process are built using ANSYS APDL software. The general modelling flow is presented as follows (**Fig.** 8):

Step1: The element type is defined as Solid185, and the mechanical properties within 25~200°C are set according to the parameters provided by the material manufacturer and calculated by the JMatPro software. The bilinear isotropic hardening model is used as the constitutive model.

Step2: The geometry of a 40×20×4 mm rectangle cuboid is established. The length, width and thickness of the FE model are all 1/5 of those of the specimen in experiments. The geometry model is divided into 20 layers (0.2mm each layer) to investigated the residual stress evolution in each depth. The FE meshing is generated by sweeping method.

Step3: The spring elements with low normal stiffness are generated around the solid elements to constrain the displacements and make the free deformation of the specimen at the same time. The normal stiffness is set as 10mm/N.

Step4: The initial residual stress field is defined layer by layer using the "inistate" function according to the stress measurement test results.

Step5: The transient mechanical and thermal loads are defined according to the actual process flow. Thermal loads are applied according to the temperature-time curve measured in experiments. Periodic displacement boundary conditions are defined to simulate the vibration of the table and specimen, and the displacements are determined by the harmonic analysis results of SREP. The FE model is solved by the transient analysis, and the results are extracted in the post-processing.

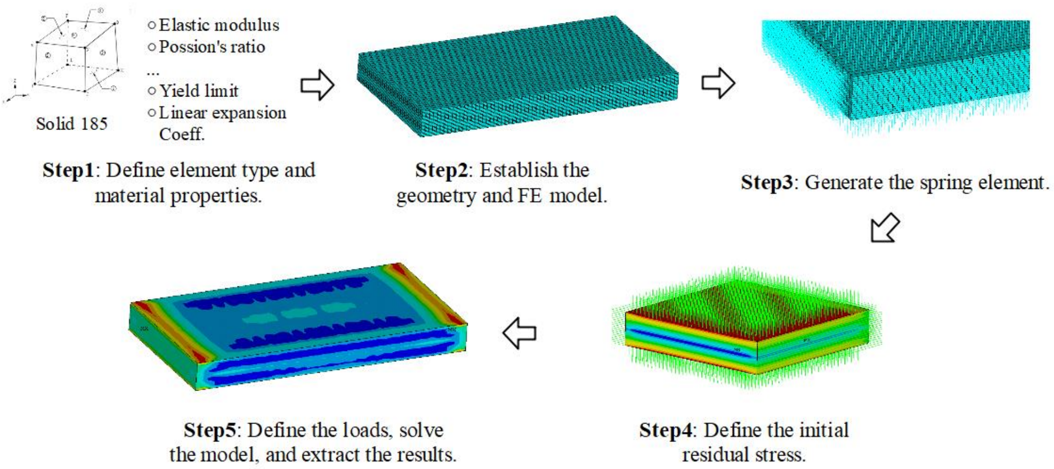

Fig. 8 General modelling flow of the stress relief process.

Thus, the residual stress evolution under the stress relief process can be acquired by solving the FE models.

2.3 Residual stress and characterization tests

As is shown in **Fig.** 9, Prism system is used to measure the residual stress in the surface (produced by Stresstech Group, Finland). Some cemented carbide micro milling cutters with 1.6mm diameter are installed to the Prism system for the hold-drilling. The high-speed camera can distinguish the strain variation caused by the hold-drilling through the laser speckle interference technique. Thus, the residual stress at different depths beneath the surface can be obtained. Two points of each specimen are measured, the point position is shown in **Fig.** S3. The measuring depths of each point are 0.02, 0.04, 0.06, 0.08, 0.1, 0.12, 0.14, 0.16, 0.18, 0.20, 0.40, 0.80 and 1.00mm.

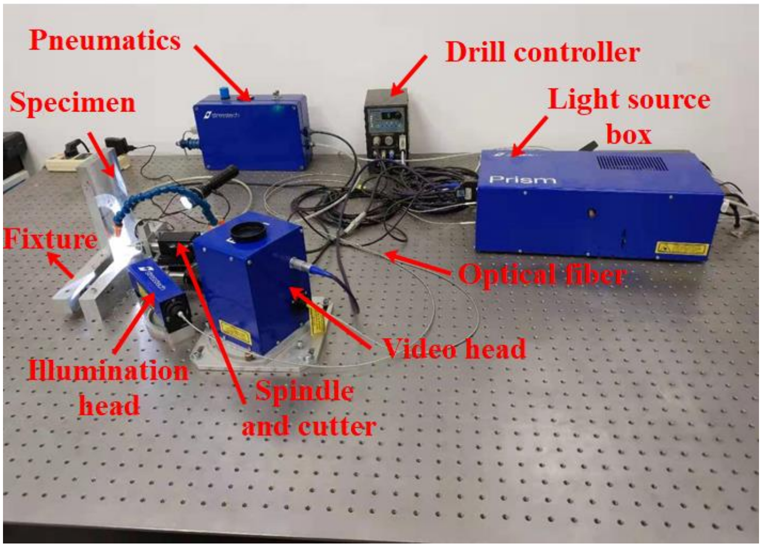

Fig. 9 Residual stress measuring experiments.

Two cuboid samples near the residual stress measuring points, whose size is 15mm×15mm×5mm, are taken from the specimen for the SEM and TEM tests (**Fig.** S3). SEM tests are conducted on SP1 and SP2, and TEM tests are conducted on SP1, SP2, SP3, SP5 and SP6. The samples are corroded before SEM test. The corrosion solution includes 40% hydrofluoric acid (HF), 69% hydroazide acid (HN_3), 30% hydrochloric acid (HCl) and water (H_2O), mixed according to 2:3:5:190. Phenom ProX (produced by Phenom-world, Netherlands) is applied for SEM characterization.

Struers TenuPol-5 automatic twin-Jet electropolisher (produced by Struers co. ltd, Denmark) is used for reduce the thickness of the sample, and JEM-2010 (produced by Japan Electronics Co., Ltd, Japan) is applied for TEM characterization.

3. Results and discussions

3.1 Residual stress

3.1.1 Stress relief effects

The measured and simulated stress results are presented in **Fig.** 10. Measured residual stresses in the length direction (*X* direction) and width direction (*Y* direction) of each specimen can be obtained by averaging the experimental data of two measuring points of each specimen (**Tabs.** S1 and S2). The simulated average value is the average stress of the objective area in FE model, and the objective area is the elements within 1mm of the upper surface. The peak value is the maximum absolute value of stress. Then, the peak and average values are used to evaluate the stress relief effects of TVSR, TSR, and VSR. The data of SP1 is considered as the original residual stress before stress relief process, because no treatment is conducted to SP1.

It shows that the simulation results have good consistency with the experimental results. The maximum absolute errors of SP2~6 are -23.64, -22.06, 15.61, 17.46, 12.84 MPa, respectively, and the maximum relative errors are 54.07%, -20.80%, 18.92%, 21.19%, and 13.36%, which validates the effectiveness and accuracy of the FE model (**Fig.** 10a and 10b).

The measured peak values in *X* direction of SP 1~6 are 143.5, -43.72, 91.50, 82.50, 67.20 and 96.10 MPa, respectively, and those in *Y* direction are 110.65, -53.05, 106.05, 76.5, 80.15, and 98MPa, respectively. The measured average values in *X* direction of SP 1~6 are 63.34, -16.06, 36.17, 35.67, 21.34, and 25.68 MPa, respectively, and those in *Y* direction are 53.01, -25.32, 34.78, 24.35, 31.12, and 35.50, respectively.

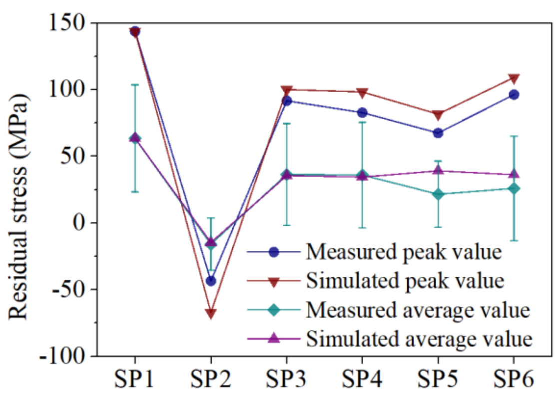

(a)

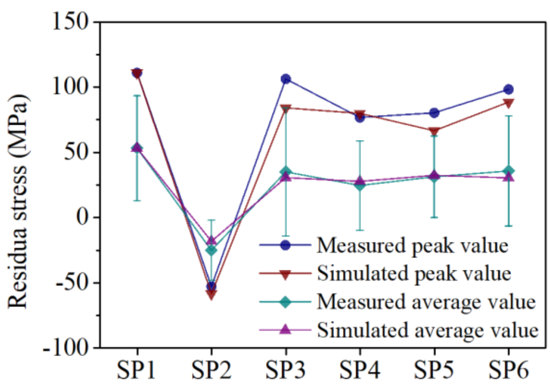

(b)

Journal Pre-proof

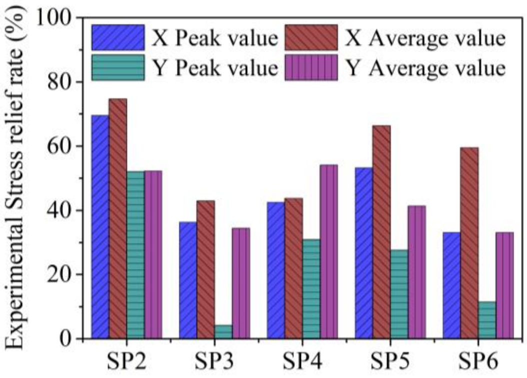

(c)

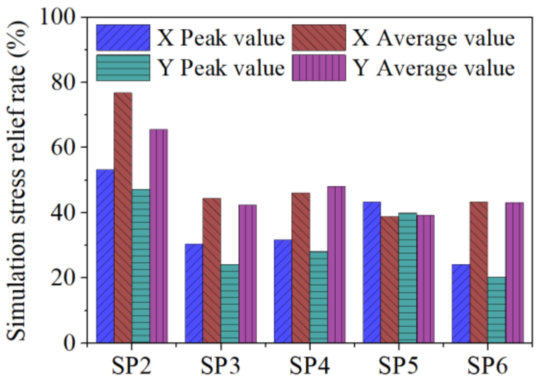

(d)

Fig. 10 Residual stress results: (a) experimental and simulation results in *X* direction, and (b) experimental and simulation results in *Y* direction, (c) experimental stress relief rate results, and (d) simulation stress relief rate results.

Averaging the stress value in *X* and *Y* directions, the stress relief rates of the peak value of SP2~SP6 are 60.79%, 20.20%, 36.69%, 40.37%, and 22.23%, respectively, and those of the average value are 63.44%m 38.64%, 48.88%, 53.80%, and 46.24%.

It shows that the stress relief rate of the peak value of TVSR (SP2) is 20.43% and 38.56% higher than that of TSR (SP5) and VSR (SP6), respectively, and the stress relief rate of the average value is 9.64% and 17.20% higher than that of TSR and VSR, respectively. Moreover, the stress relief effect of TVSR also has an advantage over TSR followed by VSR (SP3) and VSR followed by TSR (SP4), which indicates that TVSR is more effective in stress relief due to the coupling and interaction effect of heat and vibration, rather than the simple addition of them.

3.1.2 Stress evolution

The simulation stress results of the node in the geometry center at different depth are presented in **Fig.** 11, and the FEM Stress contours in *X* direction are shown in **Fig.** 12.

As is shown in **Fig.** 11a, 11b and 12a, the stress is slightly released in the heating stage, and large dynamic stress is generated in the vibration stage. The tensile stress turns into compressive stress after vibration and holding stage. This is because the specimen is clamped before heating, and the fixture limits the thermal expansion of the specimen during the heating, vibration with preservation, and preservation process. The heat and vibration during TVSR process redistribute the residual stress. The stress redistribution accompanied by limitation of the thermal expansion produces the compressive stress in the specimen, which is positive to the mechanical properties. The compressive stress slightly fluctuates in the cooling stage until the end of processing.

As is shown in **Fig.** 11c, 11d and 12b, the tensile stress does not turn into compressive stress after vibration at room temperature, but the peak value in *X* direction of the stress is decreased from 143.50MPa to 114.7MPa. The stress continues to decrease during heating and holding stages. However, the stress slightly increases due to the unstable stress state and the increase of elastic modulus and yield limit. As is shown in **Fig.** 11e, 11f and 12c, the stress continuously declines in the heating, holding, and cooling stages, and the distribution rule of the stress remains unchanged.

In summary, the periodic vibration can reduce the residual stress in a relative short time, but stress concentrations could exist at local location. Although it is the time-consuming, holding temperature for a relative long time can evenly decrease the stress magnitude. The periodic vibration at 175°C has higher stress relief effect than that at room temperature, and the following holding process as well as the clamping loads can further homogenize the stress and turn the tensile stress into compressive stress.

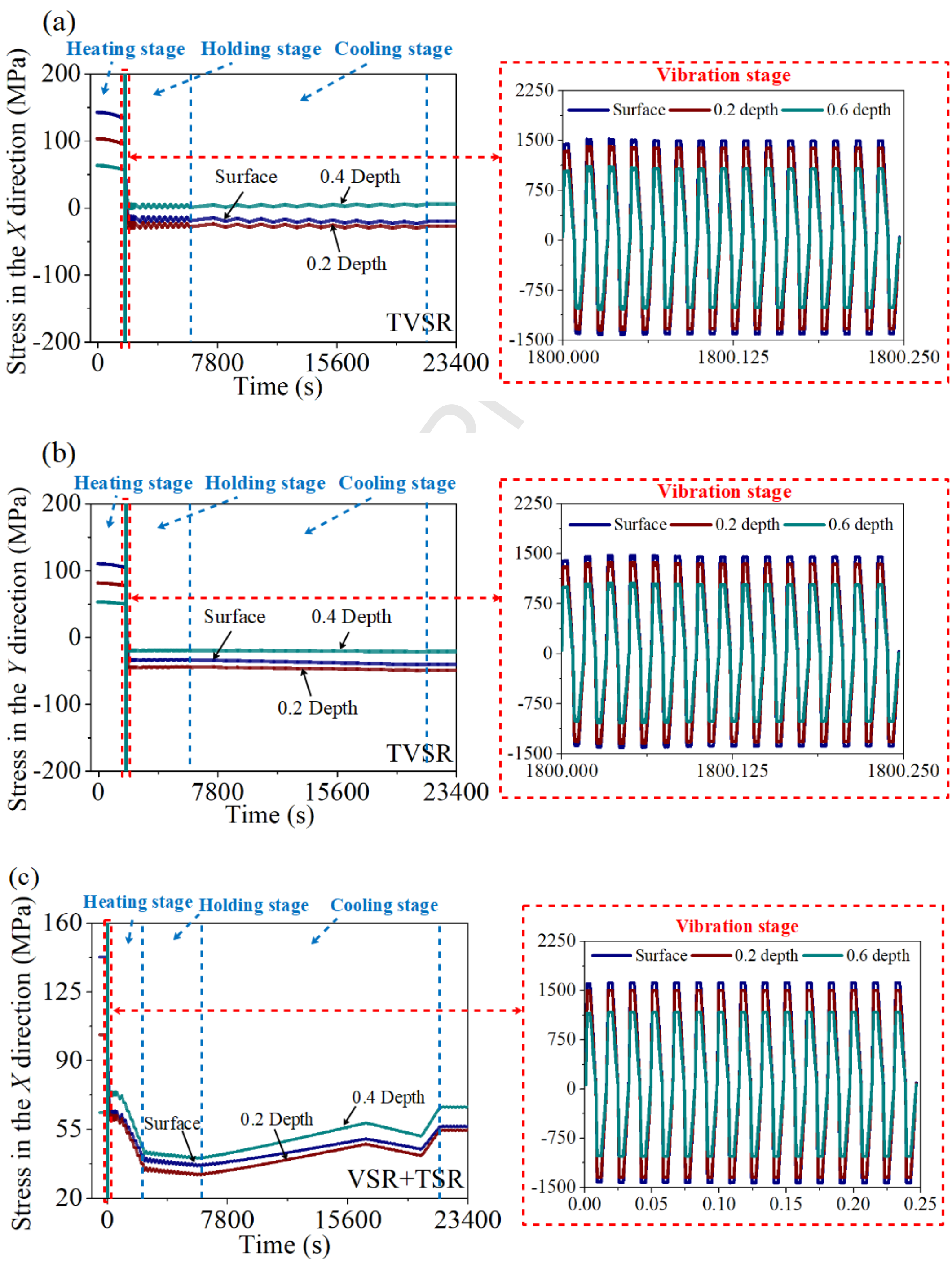

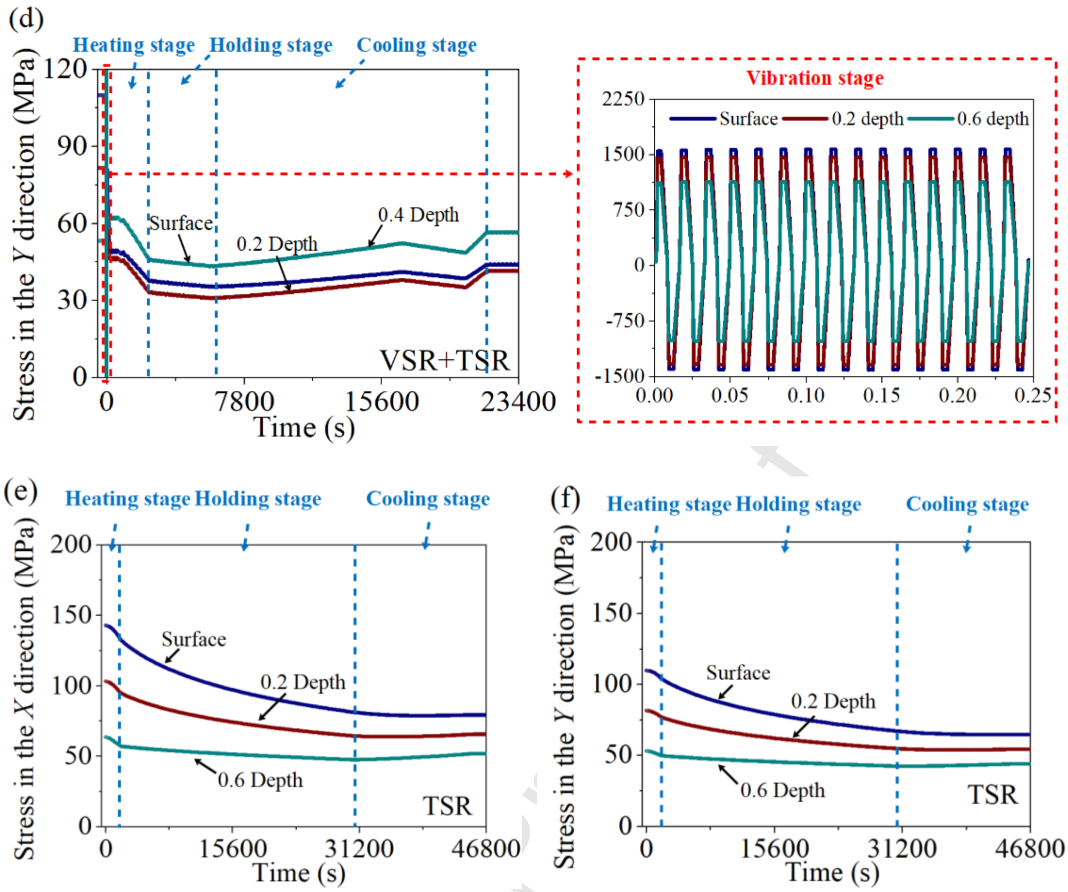

Fig. 11 FEM Stress-time curves. Stress in (a) *X* and (b) *Y* direction for SP2 (TVSR), Stress in (c) *X* and (d) *Y* direction for SP4 (VSR+TSR), and Stress in (e) *X* and (f) *Y* direction for SP5 (TSR).

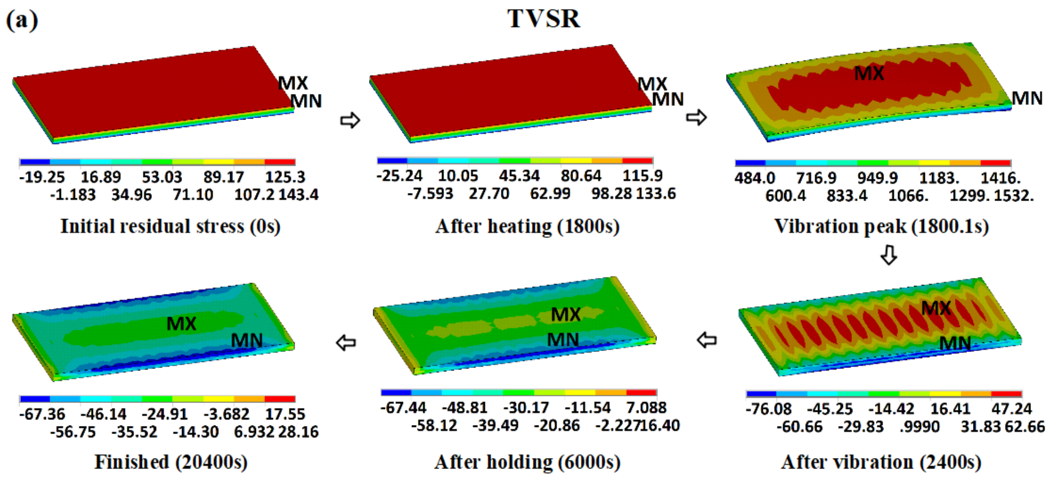

Journal Pre-proof

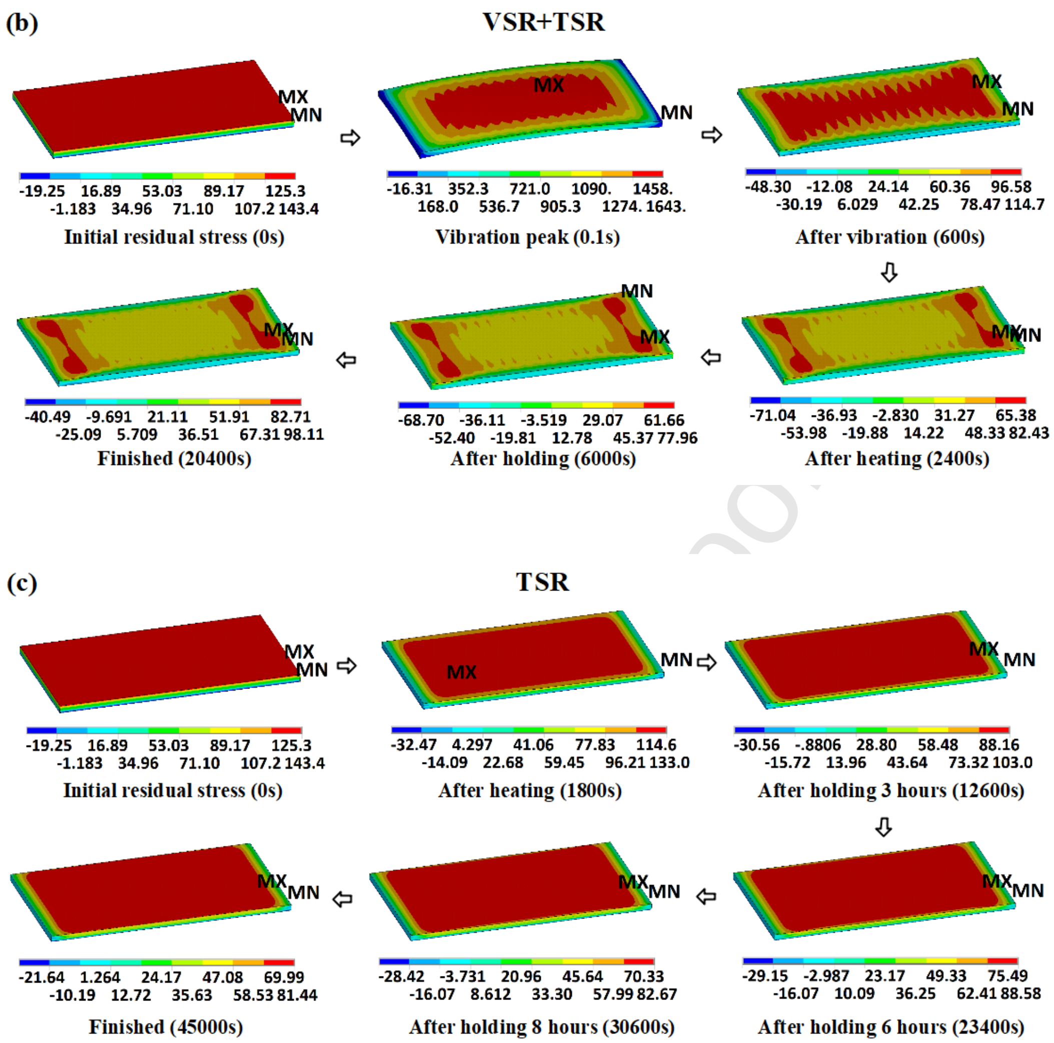

Fig. 12 FEM Stress contours in *X* direction, (a) SP2 (TVSR), (b) SP4 (VSR+TSR), and (c) SP5 (TSR).

3.2 Characterizations

The SEM micrographs of SP1and SP2 are presented in **Fig.** 13. It shows that there is no significant difference between SP1 and SP2. The grain size changes in the range of 30-300 μ m, and about 70% grains are in the range of 50-150 μm. Some coarse grains are larger than 150 μm. The coarse and the inhomogeneous grains should be caused by the uneven temperature and stress field during the forging process. It is also observed that large grains engulf small grains and grow, and some of them are elongated due to the plastic deformation. The black holes in the images are caused by the exfoliation of tiny particles in the alloy during the corrosion process. Thus, TVSR has no obvious influence on the microstructure of aluminium alloy, which is similar to that of VSR [42,46].

In actual production, workpiece deformation occurs after TSR due to the change of microstructure and grain size, and TSR is usually applied in the blank forming stage. VSR is applied before finishing or semi-finishing process due to the no significant change of the workpiece dimension after VSR. Therefore, the TVSR can be used in both blank forming and finishing or semi-finishing process for the residual stress relief, but it can't play the role of grain refinement like TSR.

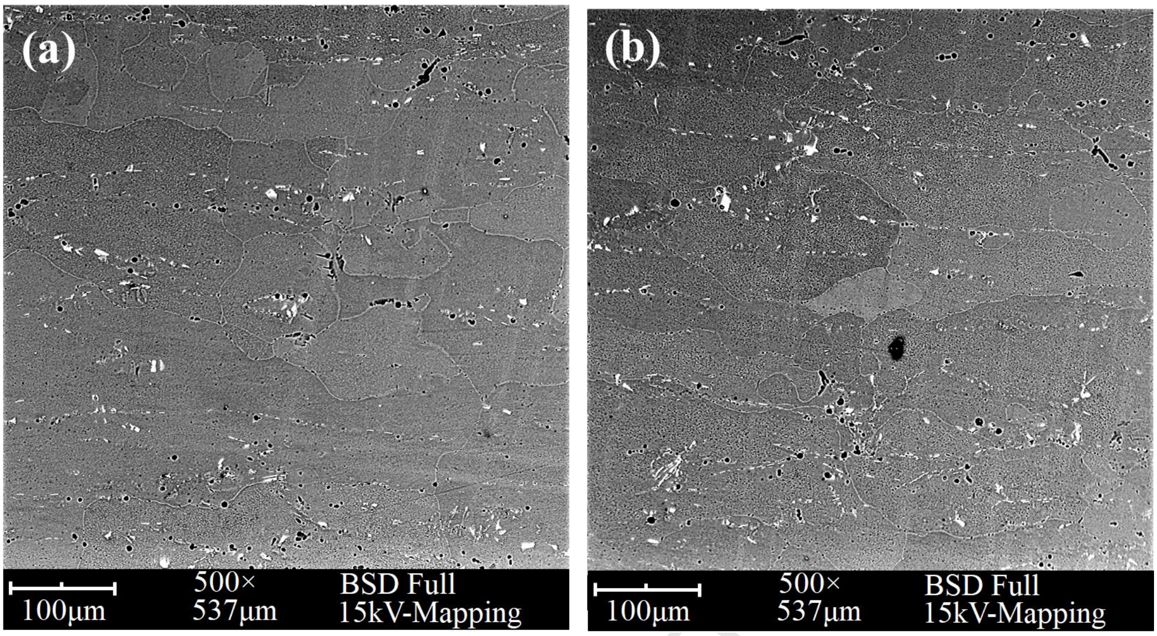

Fig. 13 Scanning electron microscope (SEM) images: (a) SP1 (No treatment), (b) SP2 (TVSR).

The TEM characterizations of SP1, SP2, SP3, SP5 and SP6 in 1-0-0 direction are shown in **Fig.** 14. The dislocations in the crystals can be observed at a magnification of 6000x and 10000x. The lines with darker color and crack shape are dislocation lines. According to **Fig.** 14, the order of dislocation density from high to low is SP6, SP3, SP2, SP1 and SP5, namely VSR ⩾ TSR before VSR > TVSR > no treatment > TSR.

Generally, when the superposition of the initial residual stress and cyclic dynamic stress in VSR exceeds the yield limit of the material, the micro plastic deformation and dislocation will be produced in the crystal, accompanying the residual stress relief. While TSR decreases the dislocation density [52]. In present study, the dislocation changes observed by TEM are consistent with the conclusions above.

In the original specimen, the dislocation density is relatively small, and there are a lot of non-activated linear dislocations. The dislocation obviously increased and intertwined into a network structure after VSR or TVSR, which shows that TVSR or VSR promotes the growth and entanglement of dislocations in 7075 aluminum alloy. In summary, the resonance increases the dislocation density, but the 175°C aging decrease it. Thus, the specimen treated by TVSR has lower dislocation density than that treated by VSR.

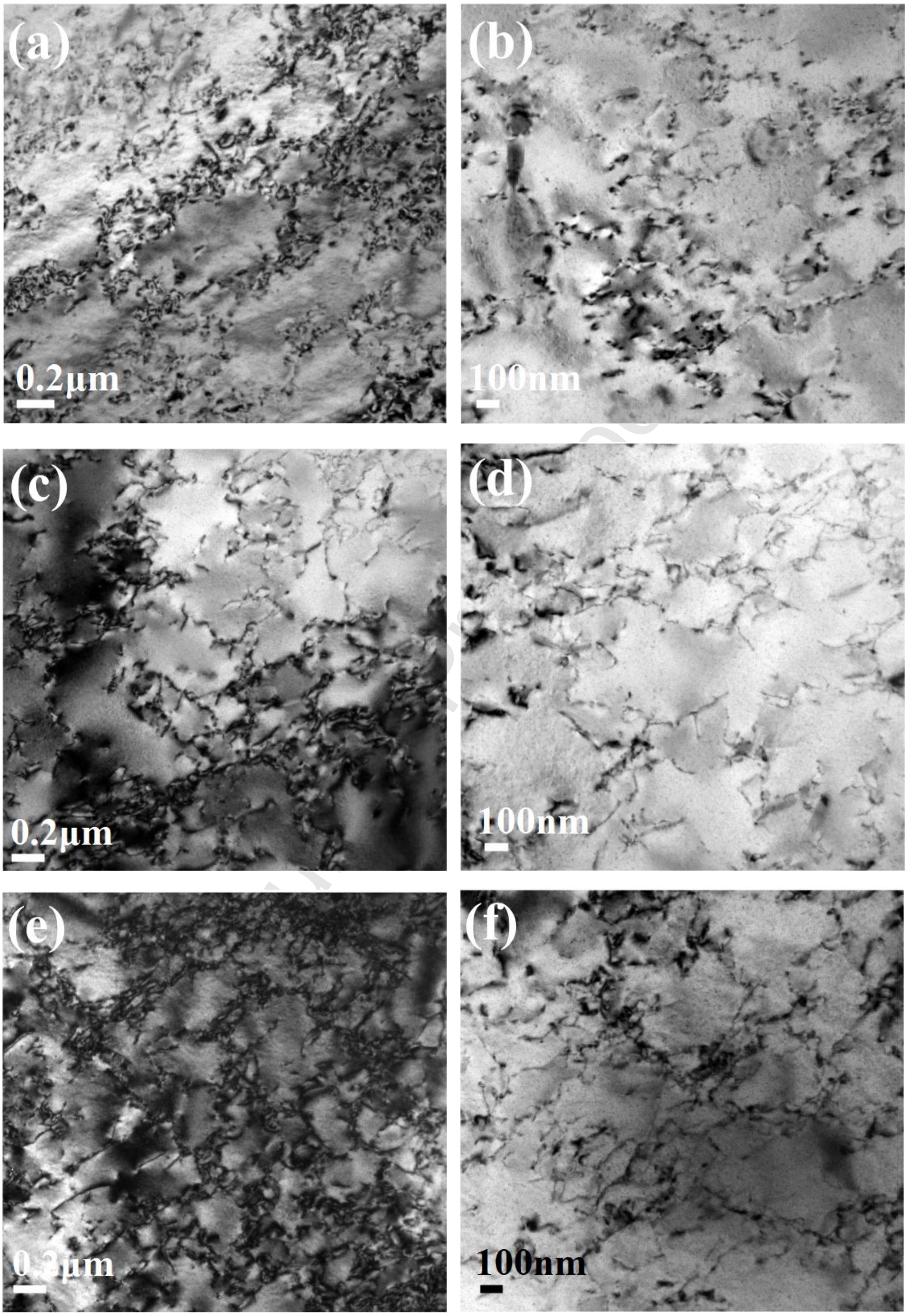
(a)
0.2μm
(b)
100nm
(c)
0.2μm
(d)
100nm
(e)
0.2μm
(f)
100nm

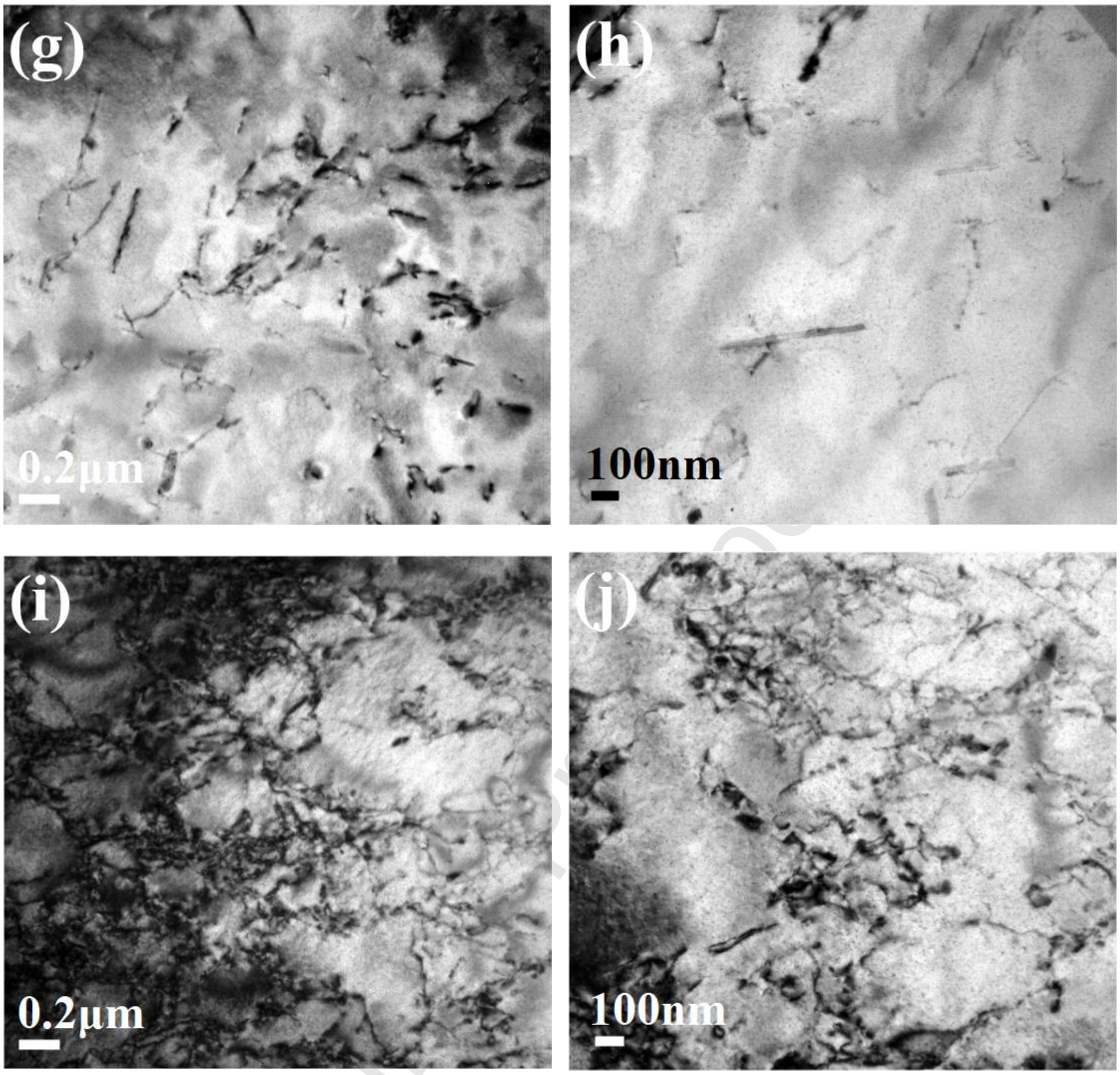

Fig. 14 1-0-0 direction transmission electron microscope (TEM) images: (a) 6000x SP1 (No treatment), (b) 10000x SP1, (c) 6000x SP2 (TVSR), (d) 10000x SP2, (e) 6000x SP3 (TSR+VSR), (f) 10000x SP3, (g) 6000x SP5 (TSR), (h) 10000x SP5, (i) 6000x SP6 (VSR), and (j) 10000x SP6.

3.3 Mechanism analysis

Except for stress relaxation at high temperature for hours, the stress relief mechanism of TSR is also explained by “softening effect”, namely the reduction of the yield limit and elastic modulus caused by the high temperature. Thus, it is easier to reach the yield limit and result in plastic deformation at high temperature [53]. However, according to the calculation results of JMatPro software (**Fig.** S4), the elastic modulus of 7075 aluminum alloy at 175°C is 6.97% lower than that at room temperature. The peak and average value of residual stress decreased by 53.17% and 66.31% after TSR. Therefore, the proportion change indicates that the stress relaxion rather than the “softening effect” is the primary stress relief cause of the TSR.

It is generally accepted by researchers that the mechanism of VSR is that the energy generated by vibration can restore the stable state of disordered lattice or interstitial atoms, and then affects the stress state. If the superposition of dynamic and initial residual stress exceeds the material yield limit, the plastic flow and micro plastic deformation will occur, and the residual stress will be released [54]. The occurrence of micro plastic deformation leads to dislocation movement and proliferation, which increases the dislocation density. While other researchers believe that the plastic flow and micro plastic deformation in the vibration process occur more easily than in static state. The stress relief is observed even if the superposition of dynamic and initial residual stress does not reach or approach the yield limit [22]. So far, there is no agreement between the two views.

Therefore, to sum up, the stress relief mechanism of TVSR can be analyzed and summarized as follows. Heat and vibration in the TVSR are not a simple addition, but a relationship of mutual promotion, compatibility and coupling (**Fig.** 15). In terms of heat promoting the vibration, the high temperature provides energy for the movement of atoms, decreases the resistance of dislocation movement, and reduces the necessary dynamic stress for micro plastic deformation. Correspondingly, in terms of vibration promoting the heat, the periodic dynamic stress accelerates the rate of stress relaxation, which makes it possible for stress relaxation to take place in a relative short period of time.

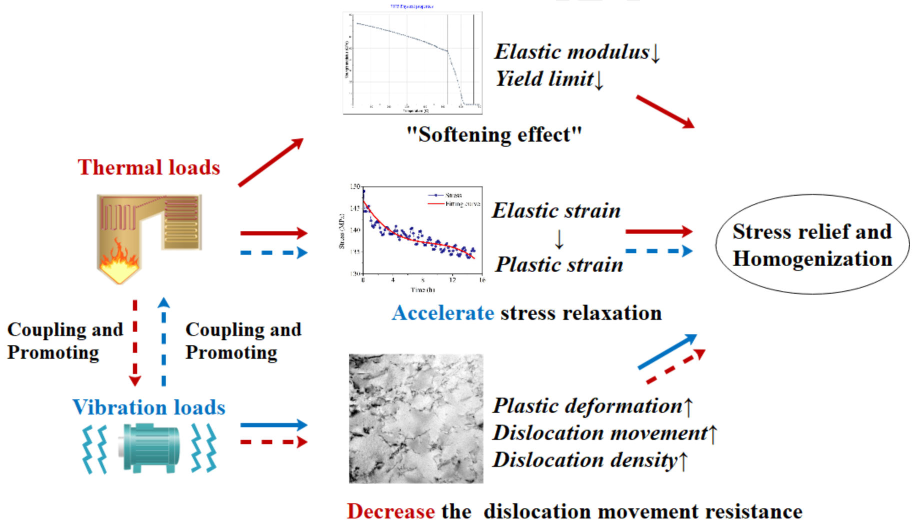

Fig. 15 Mechanism diagram of TVSR.

4. Conclusions

In this study, the 7075 aluminium alloy specimens are treated by TVSR, TSR, and VSR, and the residual stresses before and after the stress relief processes are measured and compared. FE models are established to further investigate the stress relief processes. SEM and TEM are applied to characterize the microstructure and crystal dislocation, respectively. Eventually, the influences of TVSR on the residual stress, microstructure, and crystal dislocation are analyzed. Several conclusions are drawn as follows:

(1) The simulation results of the proposed FE models have good consistency with the experimental results. The maximum absolute error of the stress is -23.64MPa.

(2) The TVSR can effectively reduce the residual stress in 7075 aluminum alloy, and the stress relief rate of TVSR for the peak stress are 20.43%, and 38.56% higher than that of TSR

and VSR.

(3) Similar to VSR, TVSR has no obvious influence on the grain size of aluminium alloy. Therefore, TVSR can be applied before finishing or semi-finishing process without changing the dimensions of the workpiece, but it can't play the role of grain refinement like TSR.

(4) TVSR or VSR promotes the growth and entanglement of dislocations in the crystals, while TSR decreases the dislocation density.

(5) The stress relief mechanism of TVSR can be explained as the mutual promotion, interaction, and coupling of the heat and vibration. The enhanced dislocation movement, accelerated stress relaxation, and the "softening effect" of the material are the main reasons of the stress relief and homogenization.

Acknowledgements

The work is financially aided by Civil Aerospace Technology Pre-research Project (B109).

References

[1] Perić M, Tonković Z, Rodić A, et al. Numerical analysis and experimental investigation of welding residual stresses and distortions in a T-joint fillet weld[J]. Materials & Design, 2014, 53: 1052-1063. doi:10.1016/j.matdes.2013.08.011.

[2] Gao H, Zhang Y, Wu Q, et al. Investigation on influences of initial residual stress on thin-walled part machining deformation based on a semi-analytical model[J]. Journal of Materials Processing Technology, 2018, 262: 437-448. doi:10.1016/j.jmatprotec.2018.04.009.

[3] Li Y, Zhou K , Tan P , et al. Modeling temperature and residual stress fields in selective laser melting[J]. International Journal of Mechanical Sciences, 2017, 136:24-35. doi: 10.1016/j.ijmecsci.2017.12.001.

[4] Zhou J Z, Huang S, Zuo L D, et al. Effects of laser peening on residual stresses and fatigue crack growth properties of Ti-6Al-4V titanium alloy[J]. Optics and Lasers in Engineering, 2014, 52: 189-194. doi:10.1016/j.optlaseng.2013.06.011.

[5] Huang K, Yang W. Analytical modeling of residual stress formation in workpiece material due to cutting[J]. International Journal of Mechanical Sciences, 2016, 114:21-34. doi: 10.1016/j.ijmecsci.2016.04.018.

[6] Gujba A , Medraj M. Laser Peening Process and Its Impact on Materials Properties in Comparison with Shot Peening and Ultrasonic Impact Peening[J]. Materials, 2014, 7(12):7925-7974. doi:10.3390/ma7127925.

[7] Vázquez J, Navarro C, Domínguez J. Experimental results in fretting fatigue with shot and laser peened Al 7075-T651 specimens[J]. International Journal of Fatigue, 2012, 40: 143-153. doi:10.1016/j.ijfatigue.2011.12.014.

[8] Zhu K, Jiang C, Li Z, et al. Residual stress and microstructure of the CNT/6061 composite

Journal Pre-proof

after shot peening[J]. Materials & Design, 2016, 107: 333-340. doi:10.1016/j.matdes.2016.06.030.

[9] Wu Q, Xie D, Jia Z, et al. Effect of shot peening on surface residual stress distribution of SiCp/2024Al[J]. Composites Part B: Engineering, 2018, 154: 382-387. doi:10.1016/S1000-9361(11)60448-2.

[10] Atig A, Sghaier R B, Seddik R, et al. Probabilistic methodology for predicting the dispersionof residual stresses and Almen intensity considering shot peening process uncertainties[J]. The International Journal of Advanced Manufacturing Technology, 2018, 94(5-8): 2125-2136. doi:10.1007/s00170-017-1033-3.

[11] Sorsa A, Santa-aho S, Wartiainen J, et al. Effect of shot peening parameters to residual stress profiles and Barkhausen noise[J]. Journal of Nondestructive Evaluation, 2018, 37(1): 10. doi:10.1007/s10921-018-0463-7.

[12] Ghasemi A, Hassani-Gangaraj S M, Mahmoudi A H, et al. Shot peening coverage effect on residual stress profile by FE random impact analysis[J]. Surface Engineering, 2016, 32(11): 861-870. doi:10.1080/02670844.2016.1192336.

[13] Mahmoudi, A.H, Ghasemi, A, Farrahi, G.H, et al. A comprehensive experimental and numerical study on redistribution of residual stresses by shot peening[J]. Materials & Design, 2015, 90:478-487. doi:10.1016/j.matdes.2015.10.162.

[14] Tan L, Zhang D, Yao C, et al. Evolution and empirical modeling of compressive residual stress profile after milling, polishing and shot peening for TC17 alloy[J]. Journal of Manufacturing Processes, 2017, 26: 155-165. doi:10.1016/j.jmapro.2017.02.002.

[15] Sherafatnia K, Farrahi G H, Mahmoudi A H. Effect of initial surface treatment on shot peening residual stress field: Analytical approach with experimental verification[J]. International Journal of Mechanical Sciences, 2018, 137: 171-181. doi:10.1016/j.ijmecsci.2018.01.022.

[16] Martín V, Vázquez J, Navarro C, et al. Effect of shot peening residual stresses and surface roughness on fretting fatigue strength of Al 7075-T651[J]. Tribology International, 2020, 142: 106004. doi:10.1016/j.triboint.2019.106004.

[17] Bagherifard S , Fernandezpariente I , Ghelichi R , et al. Effect of severe shot peening on microstructure and fatigue strength of cast iron[J]. International Journal of Fatigue, 2014, 65:64-70. doi:10.1016/j.ijfatigue.2013.08.022.

[18] Trsko L , Bokuvka O , Novy F , et al. Effect of severe shot peening on ultra-high-cycle fatigue of a low-alloy steel[J]. Materials & design, 2014, 57(may):103-113. doi:10.1016/j.matdes.2013.12.035.

[19] Hassani-Gangaraj SM, Cho KS, Voigt HJL, et al. Experimental assessment and simulation of surface nanocrystallization by severe shot peening[J]. Acta Materialia, 2015, 97:105-115. doi:10.1016/j.actamat.2015.06.054.

[20] Ahmad B, Fitzpatrick M E. Analysis of residual stresses in laser-shock-peened and

shot-peened marine steel welds[J]. Metallurgical and Materials Transactions A, 2017, 48(2): 759-770. doi:10.1007/s11661-016-3867-y.

[21] Chen M, Liu H, Wang L, et al. Evaluation of the residual stress and microstructure character in SAF 2507 duplex stainless steel after multiple shot peening process[J]. Surface and Coatings Technology, 2018, 344: 132-140. doi:10.1016/j.surfcoat.2018.03.012.

[22] Sun R, Li L, Zhu Y, et al. Microstructure, residual stress and tensile properties control of wire-arc additive manufactured 2319 aluminum alloy with laser shock peening[J]. Journal of Alloys and Compounds, 2018, 747: 255-265. doi:10.1016/j.jallcom.2018.02.353.

[23] Coules H E, Colegrove P, Cozzolino L D, et al. Effect of high pressure rolling on weld-induced residual stresses[J]. Science and Technology of Welding and Joining, 2012, 17(5): 394-401. doi:10.1179/1362171812Y.0000000021.

[24] Zhang M, Deng J, Liu Z H, et al. Investigation into contributions of static and dynamic loads to compressive residual stress fields caused by ultrasonic surface rolling [J]. International Journal of Mechanical Sciences, 2019, 163: 105144. Doi: 10.1016/j.ijmecsci.2019.105144.

[25] Colegrove P A, Coules H E, Fairman J, et al. Microstructure and residual stress improvement in wire and arc additively manufactured parts through high-pressure rolling[J]. Journal of Materials Processing Technology, 2013, 213(10): 1782-1791. doi:10.1016/j.jmatprotec.2013.04.012.

[26] Beghini M, Bertini L, Monelli B D, et al. Experimental parameter sensitivity analysis of residual stresses induced by deep rolling on 7075-T6 aluminium alloy[J]. Surface and Coatings Technology, 2014, 254: 175-186. doi:10.1016/j.surfcoat.2014.06.008.

[27] Rahimi S, King M, Christian D. Stress relaxation behaviour in IN718 nickel based superalloy during ageing heat treatments[J]. Materials Science and Engineering: A, 2017, 708: 563-573. doi:10.1016/j.msea.2017.09.116.

[28] Zeng L, Bieler T R. Effects of working, heat treatment, and aging on microstructural evolution and crystallographic texture of α, α′, α″ and β phases in Ti-6Al-4V wire [J]. Materials Science & Engineering A, 2015, 392(1):403-414. doi:10.1016/j.msea.2004.09.072.

[29] Luo K, Zang B, Fu S, et al. Stress/strain aging mechanisms in Al alloys from first principles[J]. Transactions of Nonferrous Metals Society of China, 2014, 24(7):2130-2137. doi:10.1016/S1003-6326(14)63323-9.

[30] Sun Y, Jiang F, Zhang H, et al. Residual stress relief in Al–Zn–Mg–Cu alloy by a new multistage interrupted artificial aging treatment[J]. Materials & Design, 2016, 92:281–287. doi: 10.1016/j.matdes.2015.12.004

[31] Song B, Dong S, Liu Q, et al. Vacuum heat treatment of iron parts produced by selective laser melting: Microstructure, residual stress and tensile behavior[J]. Materials & Design,

2014, 54(2):727-733. doi:10.1016/j.matdes.2013.08.085.

[32] Hönnige J R, Colegrove P A, Ahmad B, et al. Residual stress and texture control in Ti-6Al-4V wire+ arc additively manufactured intersections by stress relief and rolling[J]. Materials & Design, 2018, 150: 193-205. doi:10.1016/j.matdes.2018.03.065.

[33] Senthilkumar D. Effect of deep cryogenic treatment on residual stress and mechanical behaviour of induction hardened En 8 steel[J]. Advances in Materials & Processing Technologies, 2016, 2(4):427-436. doi:10.1080/2374068X.2016.1244326.

[34] Xu L Y, Zhu J, Jing H Y, et al. Effectsof deep cryogenic treatment on the residual stress and mechanical properties of electron-beam-welded Ti–6Al–4V joints[J]. Materials Science and Engineering: A, 2016: S0921509316308760. doi:10.1016/j.msea.2016.07.101.

[35] Ko D H, Ko D C, Hak-Jin Lim. FE-simulation coupled with CFD analysis for prediction of residual stresses relieved by cryogenic heat treatment of Al6061 tube[J]. International Journal of Precision Engineering and Manufacturing, 2013, 14(8):1301-1309. doi:10.1007/s12541-013-0177-9.

[36] Wang J.S., Hsieh C.C., Lai H.H., Kuo C.W. The relationships between residual stress relaxation and texture development in AZ31 Mg alloys via the vibratory stress relief technique. Materials Characterization.2015, 99(1):248-253. doi:10.1016/j.matchar.2014.09.019.

[37] Ebrahimi S M, Farahani M, Akbari D. The influences of the cyclic force magnitude and frequency on the effectiveness of the vibratory stress relief process on a butt welded connection[J]. The International Journal of Advanced Manufacturing Technology, 2019, 102(5-8): 2147-2158. doi:10.1007/s00170-019-03288-y.

[38] Gao H, Zhang Y, Wu Q, et al. Fatigue life of 7075-T651 aluminium alloy treated with vibratory stress relief[J]. International Journal of Fatigue, 2018, 108: 62-67. doi:10.1016/j.ijfatigue.2017.11.011.

[39] Gao H., Zhang Y., Wu Q. , et al. Experimental Investigation on the Fatigue Life of Ti-6Al-4V Treated by Vibratory Stress Relief[J]. Metals, 2017, 7(5): 158. doi:10.3390/met7050158.

[40] Gong H, Sun Y, Liu Y, et al. Effect of Vibration Stress Relief on the Shape Stability of Aluminum Alloy 7075 Thin-Walled Parts[J]. Metals, 2019, 9(1): 27. doi:10.3390/met9010027.

[41] Vardanjani M J, Ghayour M, Homami R M. Analysis of the vibrational stress relief for reducing the residual stresses caused by machining[J]. Experimental Techniques, 2016, 40(2): 705-713. doi:10.1007/s40799-016-0071-3.

[42] Mohanty S, Arivarasu M, Arivazhagan N, et al. The residual stress distribution of CO2 laser beam welded AISI 316 austenitic stainless steel and the effect of vibratory stress relief[J]. Materials Science and Engineering: A, 2017, 703: 227-235.

doi:10.1016/j.msea.2017.07.066.

[43] Shalvandi M, Hojjat Y, Abdullah A, et al. Influence of ultrasonic stress relief on stainless steel 316 specimens: A comparison with thermal stress relief[J]. Materials & Design, 2013, 46: 713-723. doi:10.1016/j.matdes.2012.11.023.

[44] Gu B, Kong D, Lai J, et al. Reduction of pulsed-laser surface irradiation induced residual stress using ultrasonic vibration method[J]. The International Journal of Advanced Manufacturing Technology, 2017, 88(1-4): 755-765. doi:10.1007/s00170-016-8798-7.

[45] Lv T, Zhang Y. 1719. A combined method of thermal and vibratory stress relief[J]. Journal of Vibroengineering, 2015, 17(6). doi: 10.21595/jve.2016.16665

[46] Li S Q, Fang H Y, Liu X S, et al. Thermal Vibration Compound Stress Relief on Thick DH36 Steel Welded Plates[C]. Applied Mechanics and Materials. Trans Tech Publications, 2014, 576: 143-147. doi:10.4028/www.scientific.net/AMM.576.143.

[47] Chen S G, Zhang Y D, Wu Q, et al. Residual Stress Relief for 2219 Aluminum Alloy Weldments: A Comparative Study on Three Stress Relief Methods[J]. Metals, 2019, 9(4): 419. doi:10.3390/met9040419.

[48] Shufen R, Dixit U S. An analysis of thermal autofrettage process with heat treatment[J]. International Journal of Mechanical Sciences, 2018, 144:134-145. Doi: 10.1016/j.ijmecsci.2018.05.053

[49] Kim D W, Cho H H, Lee W B, et al. A finite element simulation for carburizing heat treatment of automotive gear ring incorporating transformation plasticity[J]. Materials & design, 2016, 99(jun.):243-253. doi: 10.1016/j.matdes.2016.03.047

[50] Zhou J, Zhang X, Wang J. FEM simulation of stress relaxation age forming for AA7055 thin plate[J]. Ordnance Material Science and Engineering, 2013, 36(3): 98-101. doi: 10.3969/j.issn.1004-244X.2013.03.035.

[51] Lv Tian. Research on a combined method of thermal and vibratory stress relief and some key techniques [D]. Doctoral Dissertation of Beihang University, 2016, Chapter 4: 57-58.

[52] Zhang D, Niu W, Cao X, et al. Effect of standard heat treatment on the microstructure and mechanical properties of selective laser melting manufactured Inconel 718 superalloy[J]. Materials Science and Engineering: A, 2015, 644: 32-40. doi:10.1016/j.msea.2015.06.021.

[53] Shigeru Yonetani. Generation and Countermeasures of residual stress [M]. Beijing: China Machine Press, 1983. (in Chinese)

[54] Li, Shu Qi, Fang, Hong Yuan, Liu, Xue Song, et al. Relationship between the Microstructure of the Welded Steel Plates and the Efficiency of Vibration Stress Relief[J]. Advanced Materials Research, 941-944:2062-2065. doi:10.4028/www.scientific.net/AMR.941-944.2062.

Journal Pre-proof

Credit Author Statement

Hanjun Gao: Methodology, Investigation, Conceptualization, Writing-Review & Editing

Shaofeng Wu: Writing - Original Draft, Data Curation

Qiong Wu: Funding acquisition, Project administration

Bianhong Li: Formal analysis, Validation

Zihan Gao: Software

Yidu Zhang: Supervision

Shuai Mo: Resources

Journal Pre-proof

Declaration of interests

The authors declare that they have no known competing financial interests or personal relationships that could have appeared to influence the work reported in this paper.

Journal Pre-proof

Highlights:

- The influences of thermal-vibratory stress relief (TVSR), thermal stress relief (TSR), and vibratory stress relief (VSR) on the residual stress relief, micro structure, and dislocation density of 7075 aluminium alloy are investigated.
- FE models considering the stress relaxation effects and transient periodic vibration loads are proposed to simulate the TVSR, TSR and VSR process.
- The stress relief rate of TVSR for the peak stress are 20.43% and 38.56% higher than that of TSR and VSR.
- TVSR has no obvious influence on the grain size of aluminium alloy, but TVSR promotes the growth and entanglement of dislocations in the crystals.

Journal Pre-proof